Engineering Structures 33 (2011) 1195–1204

Contents lists available at ScienceDirect

Engineering Structures

journal homepage: www.elsevier.com/locate/engstruct

Preconsolidation, structural strength of soil, and its effect on subsoil upper structure interaction

Pavel Kuklík*

Czech Technical University in Prague, Faculty of Civil Engineering, 166 29 Prague, Prague 6, Czech Republic

ARTICLE INFO

Article history:
Received 15 August 2010
Received in revised form
5 November 2010
Accepted 29 December 2010
Available online 16 February 2011

Keywords:
Influence zone
Preconsolidation
Structural strength
FEM
Triaxial test
In situ testing
Deep foundation
Layered subsoil
Modified Cam clay model
Kantorovich method
Theory of convolution

ABSTRACT

When constructing a building, manufactured materials are used. That is the reason for their excellent material properties. In the case of the foundation, the natural condition of the soils must mostly always be respected. The geostatical stress plays a significant role on the subsoil behavior because it is the de facto natural form of the soil compaction. The soil has a memory of the highest stress that has ever been loaded on it. The soil can be considered incompressible if the magnitude of a surcharge is lower. In engineering practice the construction of higher buildings is founded in a deeper hole so that the depth of the influence zone achieves an acceptable value for the future surcharge of the upper structure. For very tall buildings, the deep hole foundation must be prolonged by piles. In particular, this article deals with laboratory testing that provides the preconsolidation. In Czech, we term it the structural strength of soil. The test provides the initial void ratio as well as the initial coefficient of fully saturated hydraulic conductivity. The isotropic consolidation test with the triaxial test apparatus and consequent knowledge of the pore pressure course was chosen to determine the initial soil properties, including the preconsolidation level. Derived theory together with the genetic algorithms provide an efficient tool for the determining parameters. Good knowledge of the influence zone is crucial when solving soil structure interaction. The progress of the influence zone was considered from the extensive research carried out at the University of Brasília, Brazil. Thus, using the measurements, the preconsolidation and its effect were verified in situ. The derived formulas and presented graphs for influence zone depth estimation have considerable importance for civil engineering practice. The Kantorovich method together with the strategy of convolution was used to reach dimensional reduction when deriving analytical formulas. Recommended results and formulas were verified against FEM code ADINA.

1. Introduction

It has been experimentally confirmed that a soil substantially changes its material properties when subjected to external loading. Apart from that, the soil, when subjected to a certain loading history, has the ability to memorize the highest level of loading mathematically represented by the over-consolidation ratio, and the initial void ratio. In its virgin state, the soil deformability is relatively high. In contrast, following the unloading/reloading path shows almost negligible deformation until the highest stress state the soil has ever experienced before is reached [1–3]. To study this behavior of soil, we performed several small laboratory tests. Transport processes were observed carrying out isotropic consolidation with triaxial test apparatus. Employing genetic algorithms, soil parameters were determined comparing the pore pressure course (measured and calculated) [4,5]. In the large scale, the effect of over-consolidation was simultaneously investigated by way of rigid plate and pile working diagram analysis. Both the finite element technique and elastic layer theory were employed in back analysis of the measured data. The great effect of overburden was observed on the depth of the influence zone in deep hole foundations [6,7]. This study is in general focused on the description of preconsolidation effects by self weight of overburden and on selection of the main parameters characterizing this memory of the subsoil.

2. Preconsolidation, structural strength, in laboratory testing

The test was arranged in two runs, loading/reloading. Readings were taken of the highest level of effective mean stress. Referring to experimental measurements carried out with the triaxial apparatus, the isotropic consolidation can be viewed as a one phase flow in a fully saturated deforming medium undergoing small deformation. When neglecting the body forces, the hydrostatic state of stress maintained during the experimental measurement gives

$$\sigma_x(x, y, z, t) = \sigma_y(x, y, z, t) = \sigma_z(x, y, z, t) = \sigma_m, \tag{1}$$

where σ_m is the total mean stress. Following the Terzaghi–Fillunger concept of effective stresses, this quantity can be expressed in

* Tel.: +420 2 2435 4486; fax: +420 2 2431 0775.
E-mail address: kuklikpa@fsv.cvut.cz.

0141-0296/$ – see front matter © 2011 Elsevier Ltd. All rights reserved.
doi:10.1016/j.engstruct.2010.12.041

terms of the pore pressure p^s and the effective stresses between grains σ_m^{eff} as

$$\sigma_m = \sigma_m^{\text{eff}} - p^s. \tag{2}$$

Assuming full saturation ($S_w = 1$) the pore pressure p^s equals the pressure in the liquid phase p^w. Referring to experimental conditions, the total mean stress remains constant throughout the consolidation process. The assumed stress homogeneity together with Eq. (2) then provide

$$\dot{\sigma}_m = \dot{\sigma}_m^{\text{eff}} - \dot{p}^w = 0, \tag{3}$$

where $\dot{(\cdot)}$ represents the time derivative $\partial(\,)/\partial t$. Transport of the liquid phase throughout the soil sample can be described by the following set of equations:

Transport equation

$$J^w = -\frac{K\,\rho^w}{\gamma^w} \cdot \operatorname{grad} p^w, \tag{4}$$

where J^w is the mass flux of pore water, $\gamma^w = g\rho^w$ is the specific weight of water, ρ^w is the intrinsic mass density and K represents an instantaneous coefficient of permeability.

The balance equation reads

$$\rho^w \dot{\varepsilon}_V + \operatorname{div} J^w = 0. \tag{5}$$

The volumetric strain ε_V follows from the constitutive equation

$$\varepsilon_V = \frac{e - \bar{e}_0}{1 + \bar{e}_0} = -\frac{\kappa}{1 + \bar{e}_0} \ln(-\sigma_m^{\text{eff}}),$$
$$\sigma_m^{\text{eff}} > \bar{\sigma}_m^{\text{eff}} = -p_c, \tag{6}$$
$$\varepsilon_V = \frac{e - e_0}{1 + e_0} = -\frac{\lambda}{1 + e_0} \ln(-\sigma_m^{\text{eff}}),$$
$$\sigma_m^{\text{eff}} > \bar{\sigma}_m^{\text{eff}} = -p_c, \tag{7}$$

they were derived for the case of the modified Cam clay model from the bilinear consolidation line, Fig. 1. Actual void ratio is denoted by e. The initial branch, often referred to as κ-line, gives evidence of the previous stress history and represents the effect of preconsolidation. The slope discontinuity between the κ and λ-lines can be identified with the structural strength of the soil given in terms of a certain level of the effective mean stress $\bar{\sigma}_m^{\text{eff}} = -p_c$ (p_c is termed the preconsolidation pressure). Initial void ratios for the κ and λ-lines are $\bar{e}_0$, e_0 respectively. Differentiating Eq. (7) with respect to time gives the rate of volumetric strain in the form

$$\dot{\varepsilon}_V(t) = \frac{\dot{e}}{1 + e_0} = -\frac{\lambda}{1 + e_0} \frac{\dot{p}^w}{\sigma_m^{\text{eff}}}. \tag{8}$$

Substituting Eqs. (4) and (8) into Eq. (5) and taking into account the actual triaxial set-up, in which only the bottom face of the cylinder is drained, leads to

$$-\frac{1 + e_0}{\gamma^w \lambda} \sigma_m^{\text{eff}}(z,t) \frac{\partial}{\partial z}\left(K(z,t) \frac{\partial p^w(z,t)}{\partial z}\right) - \dot{p}^w(z,t) = 0. \tag{9}$$

It has been verified experimentally that in the case of isotropic consolidation a simple power law written as (more in [8–11])

$$\frac{K(z,t)}{K_0} = \left(\frac{e(z,t)}{e_0}\right)^m, \tag{10}$$

represents the soil behavior fairly well. The dependence of the actual void ratio e on the effective mean stress, Eq. (7), together with Eq. (10) provide

$$\frac{\partial K(z,t)}{\partial z} = -\frac{mK(z,t)\lambda}{e(z,t)\,\sigma_m^{\text{eff}}(z,t)} \frac{\partial p^w(z,t)}{\partial z}. \tag{11}$$

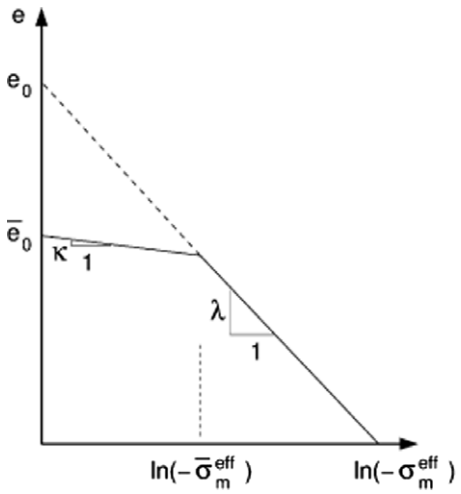

Fig. 1. Bilinear form of the normal consolidation line.

Introducing Eq. (11) into Eq. (9) finally yields.

$$\dot{p}^w(z,t) = -\frac{K(z,t)(1+e_0)}{\gamma^w \lambda}\left[-\frac{m\lambda}{e(z,t)}\left(\frac{\partial p^w(z,t)}{\partial z}\right)^2 + \sigma_m^{\text{eff}}(z,t)\frac{\partial^2 p^w(z,t)}{\partial z^2}\right]. \tag{12}$$

A similar equation can be derived for the unloading branch when replacing λ by κ and e_0 by $\bar{e}_0$ in Eq. (12)

$$\dot{p}^w(z,t) = -\frac{K(z,t)(1+\bar{e}_0)}{\gamma^w \kappa}\left[-\frac{m\kappa}{e(z,t)}\left(\frac{\partial p^w(z,t)}{\partial z}\right)^2 + \sigma_m^{\text{eff}}(z,t)\frac{\partial^2 p^w(z,t)}{\partial z^2}\right]. \tag{13}$$

The main objective of these steps is to introduce a simple yet accurate numerical technique for extracting material parameters of clayey soils that behave according to the Cam clay model, from a simple one-dimensional consolidation test. To introduce this task, recall that reproducing laboratory data requires supplying the *structural strength parameter* p_c, the *initial void ratio* $\bar{e}_0$, the *initial coefficient of permeability* K_0, the swelling index κ and the compression index λ. The last two material parameters and the starting value of preconsolidation pressure could be specified from the steady state response corresponding to the diagram shown in Fig. 1. This however, would require carrying out a number of isotropic consolidation tests for several predefined levels of isotropic pressures attained at the end of the consolidation process while measuring at the same time the change in volumetric strain $\Delta\varepsilon_V$. Such an approach would become not only time consuming but also would be burdened by an additional experimental error associated with the difficulty of measuring $\Delta\varepsilon_V$ and the determination of $\bar{e}_0$ and K_0 would require additional laboratory tests. In addition a trial and error method would have to be used to determine the remaining parameter m.

A simple solution avoiding such difficulties is offered by following the steps of mixed experimental and numerical methods. In such a case, combining the experimental measurements and numerical computations in a suitable optimization environment (more in [12]) provides an efficient tool for inferring the desired parameters from a single laboratory test. In particular, matching experimentally obtained data with those derived numerically might be the simplest view on a complex optimization procedure that provides the desired results.

Table 1
Optimal material parameters.

κ	λ	$\bar{e}_0$	K_0 (m s^{-1})	p_c (kPa)	m
0.012	0.074	0.56	$1.53e^{-9}$	28.45	4.7

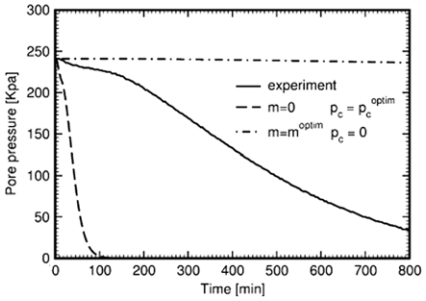

Fig. 2. Time variation of pore pressure.

To that end, recall Eq. (12) describing the excess pore pressure variation during consolidation. In view of the optimization problem, the used material and structural strength parameters $\bar{e}_0$, K_0, κ, λ, p_c, m now become the search variables to be found by minimizing the following objective function

$$F = \sum_{k=1}^{\kappa} (p^w(t_k) - \bar{p}^w(t_k))^2.$$

The minimization problem is solved with an optimization procedure called the augmented (or parallel) simulated annealing (AUSA) which efficiently combines the essentials of genetic algorithms (a population of possible solutions rather than a single solution) with the basic concept of simulated annealing. The genetic algorithm cycle consists of reproduction, recombination and selection of a new population of input parameters in which the common "cross-breeding" and "mutation" operators are randomly employed. The principle of simulated annealing is used to reduce the probability of replacing an existing individual solution by a worse one. Thus the method searches the space more evenly in the first steps and continues to concentrate in local minimums as it proceeds. The limits of the solution space correspond to minimum and maximum acceptable values of input parameters and were adopted from the literature.

In keeping up with the general scheme of the paper, we will limit our attention to two essential parameters, namely the preconsolidation pressure p_c representing the loading history and the exponent m affecting the time variation of the coefficient of permeability, Eq. (10) (details in [4,11,13]).

To derive a robust numerical procedure, the optimal parameters were sought comparing numerical data with measured values of pore pressure. An example of the result is listed in Table 1.

The influence of the preconsolidation p_c and the influence of the parameter m, describing the change of the permeability coefficient, are clearly presented in Fig. 2. Finally, the proposed theory is highlighted in Fig. 3. It is seen that the theoretical and measured loading/reloading curves fit fairly well (all details in [4]).

3. Validation of preconsolidation in situ and its testing

The pre-designed Brazilian capital Brasília, located in the Federal District of Brazil, was designed to house only the main Governmental administrative institutions and its public employees. Nevertheless, it has increased four times more than what was initially forecast and is still expanding. Construction is advancing through distinct (geological) zones of this same district, and allows the use of distinct techniques for deep foundation deployment and design.

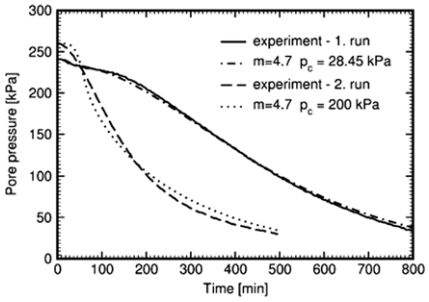

Fig. 3. Time variation of pore pressure.

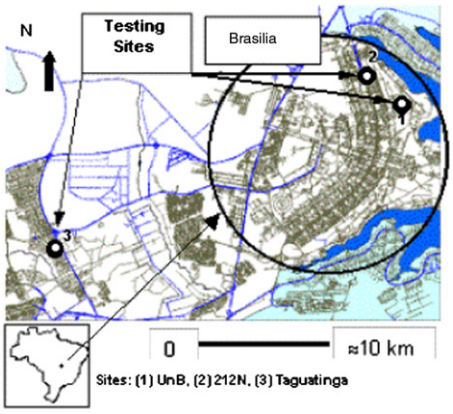

Fig. 4. Location of the studied sites.

Hence in 1995, the University of Brasília (UnB) started a major research project in order to enhance knowledge on the behavior of the typical deep foundations that are in the stratified, tropical subsoil of the Federal District. It was decided to carry out horizontal and vertical field loading tests on locally used foundation types. These foundations had full-scale dimensions and were placed within the University of Brasília campus at the experimental research site of the Geotechnical Post-Graduation Program. The geotechnical profile of this campus is composed of the typical unsaturated "porous" clay of Brasília. In addition, field loading tests on full-scale instrumented foundations outside the campus were also carried out. In all cases, the tests were performed with the cooperation of local engineering companies and University staff (Fig. 4).

A mechanically bored pile founded in the University of Brasília campus (UnB research site) is analyzed together with instrumented piles from two other engineering sites within this same district (Table 2).

One of them is a continuous flight auger type pile located in the North Wing of Brasília (212N site), close to the University Campus, and founded in the same geological material. The other is a mechanically bored pile excavated with bentonite mud, located in a site around 25 km from the University Campus (Taguatinga site), and founded in a foliated and stratified material which originates from slate decomposition.

The experimental curves of pile load versus displacement, structural load transfer along the pile's shaft, and average skin friction and base pressure versus loading level are presented and compared to numerical predictions made from a semi-analytical procedure. This procedure is coded in the industrial software denominated GEO4 Pile modulus that was developed in cooperation between the Department of Mechanics, Faculty of Civil Engineering, CTU in Prague and Fine Ltd. Software Company.

The results of back analysis are depicted in Figs. 5 and 6. The necessity for a further refinement for both 212N and Taguatinga

Table 2
General geotechnical parameters of the UnB site [14].

Parameter	Unit	Range
Sand percentage	%	12–27
Silt percentage	%	8–36
Clay percentage	%	80–37
Dry unit weight	kN/m^3	10–17
Natural unit weight	kN/m^3	17–19
Moisture content	%	20–34
Degree of saturation	%	50–86
Void ratio	–	1.0–2.0
Liquid limit	%	25–78
Plastic limit	%	20–34
Plasticity index	%	5–44
Drained cohesion[a]	kPa	10–34
Drained friction angle[a]	degrees	26–34
Young's modulus[b]	MPa	1–8
Coefficient of collapse	%	0–12
Coeff. earth press (K_0)[c]	–	0.44–0.54
Coeff. permeability	cm/s	10^{-6}–10^{-3}

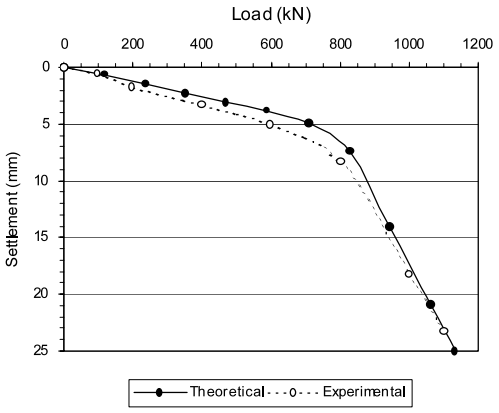

Fig. 5. Working diagram 212N pile.

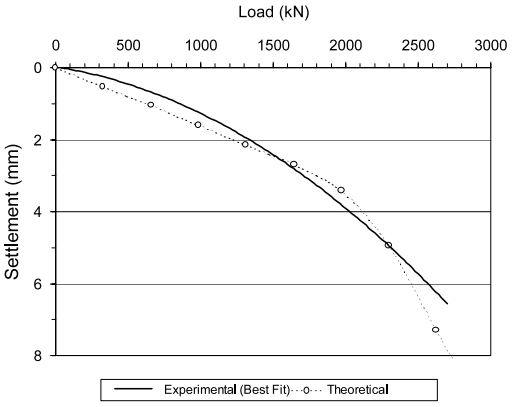

Fig. 6. Working diagram Taguatinga pile.

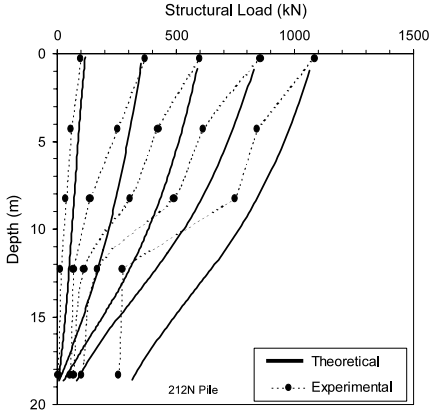

Fig. 7. Load transfer curve 212N pile.

analyses is evident when comparing the load transfer curves of these same sites, as is respectively done in Figs. 7 and 8. Hence, although refinement is required, the results can be already considered suitable from a practical point of view, if one accepts as valid and within tolerable range (in engineering terms) the errors involved in this first series of analyses (Table 3).

Fig. 8 presents the comparison of load transfer curves for the Taguatinga pile. It indicates that a fairly good result was obtained, and a better (that is than the 212N pile) agreement was achieved. Similarly as before, one can affirm that the analyses can be already considered as valid from a practical point of view. Indeed, the comparison of the average unit skin friction and the percentage of base load between numerical and experimental values is good. It is observed that, for the failure condition (3200 kN), ≈42% of the applied load at the pile's head was transmitted to the base of this pile (numerical prediction).

At working conditions (1600 kN) however, the software has estimated that ≈11% of the applied load at the pile's head would

Table 3
Back analyzed geotechnical parameters from all sites via GEO4 software.

Sublayer type	Depth (m)	Geotechnical parameter				N^*(SPT)
		ϕ' (deg)	c' (kPa)	E (MPa)	K	
UnB site:						
Clay I	0–3	27	13	5	0.6	3
Clay II	3–8	27	14	13	0.6	4
Clay III	8–12	27	52	19	0.6	4–15
Rock	>12	(Non deformable)				
212N site:						
Embankment	0–4	25	0	25	0.4	9
Clay A	4–8	27	15	20	0.4	9–5
Clay B	8–15	27	5	40	0.4	5–15
Clay C	15–25	27	5	100	0.4	15–20
Rock	>25	(Non deformable)				
Taguatinga site:						
SClay	0–2.5	27	15	20	0.7	6
CSand	2.5–5	30	10	60	0.7	10
SSilt I	5–10	30	20	120	0.7	16–40
SSilt II	10–15	40	30	600	0.7	50+
Rock	>15	(Non deformable)				

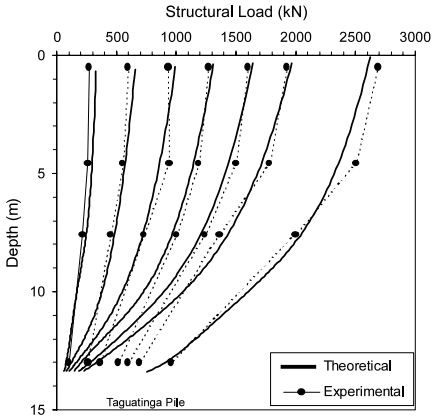

Fig. 8. Load transfer curve Taguatinga pile.

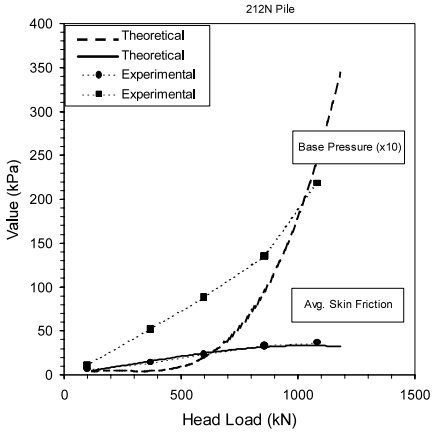

Fig. 9. Comparative results 212N pile.

be transmitted to the base of this pile. Also at this latter condition, the comparison of average unit skin friction between numerical (≈56 kPa) and experimental (≈40 kPa) values were reasonably good.

This value is very close to the value that has been experimentally measured throughout the test (as given before, around 40%).

The discrepancies are again related to the fact that the pile was founded in a very hard soil stratum (saprolite), which was not perfectly simulated in this first analysis.

The lack of agreement for the base pressure is directly related to the fact that the analyses failed to properly model the last layer or the foundation layer, where extremely high values of unit pressures took place and were indirectly measured. In numerical terms, a unique and particular soil spring was assigned to this last layer. Since it is evident from Figs. 9 and 10 (in particular the latter one) that the numerically predicted base pressures were substantially lower than the measured values, one can conclude that the stiffness of this spring was not properly incorporated in the analyses. A fine readjustment of the stiffnesses for both situations, increasing towards more representative values, would certainly improve the matching quality of the load transfer curves of Figs. 9 and 10, especially at the deepest pile sections. The experience gained with these analyses has demonstrated that deep strata, stiffer than the overlying layers and leveled to the pile's base, shall be incorporated in the numerical back analysis. This holds particularly true for the Taguatinga site, where the pile was founded on a hard saprolite medium. There was also realised the importance of having instrumented piles at the site. Although such efforts may increase construction costs, the assistance of the

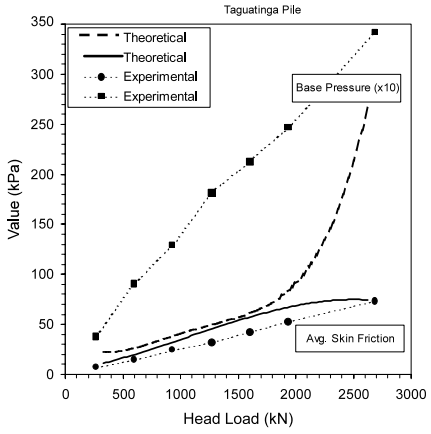

Fig. 10. Comparative results Taguatinga pile.

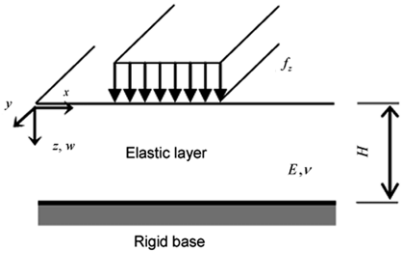

Fig. 11. Formulation of the elastic layer solution.

instrumentation in guiding and benchmarking the back analysis is of major importance (more information in [14,15]).

4. Elastic layer theory, basic ideas of dimensional reduction

The aim of the analytical solution is to determine the deformation of an elastic layer in the vertical direction. The solution procedure builds upon neglecting the horizontal displacements similar to standard assumptions applied to the analysis of Westergard subspace. Clearly, such an assumption results in a stiffer soil response thereby providing an upper estimation of the depth of influence zone. The problem formulation is evident from Fig. 11. Referring to the Kantorovich method (details in [16,17]) the distribution of the displacement field is obtained in the form

$$w(x;y;z) = \sum_{j=1,3,5}^{\infty} w_j(x;y)\psi_j(z),$$

$$\psi_j(z) = \cos\frac{j\pi}{2H}z, \tag{14}$$

where the functions $\psi_j(z)$, $j = 1, 3, 5, \ldots$ represent a complete set of base functions. Let us calculate the components of the small strain tensor. The small strain tensor is the symmetrical part of the gradient matrix tensor. From (14), it yields:

$$\varepsilon_{xx} = 0, \qquad \varepsilon_{yy} = 0, \qquad \varepsilon_{zz} = \sum_{j=1,3,5}^{\infty} w_j\psi_{j,z},$$

$$\gamma_{xy} = 2\varepsilon_{xy} = 0, \qquad \gamma_{yz} = 2\varepsilon_{yz} = \sum_{j=1,3,5}^{\infty} w_{j,y}\psi_j, \tag{15}$$

$$\gamma_{zx} = 2\varepsilon_{zx} = \sum_{j=1,3,5}^{\infty} w_{j,x}\psi_j.$$

Notation $\frac{\partial w_j}{\partial x} = w_{j,x}$ is used for the partial derivative.

For the stress–strain relation, Hooke's law is adopted:

$$\sigma_{xx} = \frac{v}{1-v}E_{\text{oed}} \sum_{j=1,3,5}^{\infty} w_j \psi_{j,z},$$
$$\sigma_{yy} = \frac{v}{1-v}E_{\text{oed}} \sum_{j=1,3,5}^{\infty} w_j \psi_{j,z}, \qquad \sigma_{zz} = E_{\text{oed}} \sum_{j=1,3,5}^{\infty} w_j \psi_{j,z},$$
$$\tau_{xy} = G\gamma_{xy} = 0, \qquad \tau_{yz} = G \sum_{j=1,3,5}^{\infty} w_{j,y} \psi_j, \tag{16}$$
$$\tau_{zx} = G \sum_{j=1,3,5}^{\infty} w_{j,x} \psi_j.$$

Symbols E, v, E_{oed}, G represent known values of Young's modulus, Poisson's ratio, oedometric modulus and shear modulus, respectively. Lagrange's principle of virtual work for the general principle of equilibrium is used in the following form:

$$\int_{R^2} \left(\int_0^H \left(G \frac{\partial w}{\partial x} \frac{\partial \delta w}{\partial x} + G \frac{\partial w}{\partial y} \frac{\partial \delta w}{\partial y} + E_{\text{oed}} \frac{\partial w}{\partial z} \frac{\partial \delta w}{\partial z} \right) \mathrm{d}z - f_z(x,y)\delta w(x,y,0) \right) \mathrm{d}x\mathrm{d}y = 0. \tag{17}$$

Since the virtual functions δw will be used in the same form as w, integrating the equilibrium equation in the vertical direction takes the form of an infinite number of partial differential equations:

$$-\Delta w_j(x,y) + (j\alpha)^2 w_j(x,y) = \frac{2}{GH} f_z(x,y), \quad j = 1,3,5,\ldots,$$
$$\alpha = \frac{\pi}{2H}\sqrt{\frac{E_{\text{oed}}}{G}} = \frac{\pi}{2H}\sqrt{\frac{2-2v}{1-2v}}. \tag{18}$$

In the case of axisymmetry or if the uniform load is acting on an infinite strip, the solution can be discovered by solving the system of ordinary differential equations. Otherwise, the strategy of convolution must be employed. Eq. (18) is the generalized form of the known Pasternak solution of subsoil (see e.g. [8,18,10,19]).

The solution of the partial differential equation can be written as the convolution of the right hand side and the fundamental solution F_j corresponding to the left hand side

$$w_j(x,y) = \frac{2}{GH} \int_{R^2} f_z(\xi,\eta) F_j(\xi - x, \eta - y)\mathrm{d}\xi\,\mathrm{d}\eta = \frac{2f_z}{GH} \int_{R^2} F_j(\xi - x, \eta - y)\mathrm{d}\xi\,\mathrm{d}\eta. \tag{19}$$

The function F_j satisfies the equation

$$-\Delta F_j + (j\alpha)^2 F_j = 0 \quad \text{for } x^2 + y^2 > 0. \tag{20}$$

It is of the form

$$F_j = \frac{1}{2\pi} K_0(j\alpha\sqrt{x^2+y^2})$$

where $K_0(j\alpha\sqrt{x^2+y^2})$ is the modified Bessel function of zero order (see [9,16]). Due to singularity of F_j at $[0,0]$ satisfies the right hand side of (19) and is evaluated as the limit of integrals over the smaller region $\Omega_\varepsilon = \Omega \setminus K_\varepsilon$ for $\varepsilon \to 0$, where K_ε is the small ball of a small positive radius ε and the center at the point $[x,y]$. Integrating (20) over and applying Green's theorem we can write

$$\int_{\Omega_\varepsilon} F_j(\xi - x, \eta - y)\mathrm{d}\xi\,\mathrm{d}\eta = \frac{1}{(j\alpha)^2} \int_{\Omega_\varepsilon} \Delta F_j(\xi - x, \eta - y)\mathrm{d}\xi\,\mathrm{d}\eta = \frac{1}{(j\alpha)^2} \oint_{\partial\Omega_\varepsilon} \left(\frac{\partial F_j}{\partial \xi}\mathrm{d}\eta - \frac{\partial F_j}{\partial \eta}\mathrm{d}\xi \right). \tag{21}$$

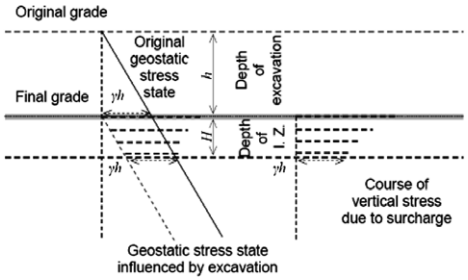

Fig. 12. The governing idea of the influence zone calculation.

If $[x,y]$ is not a point of $\partial\Omega$, $\partial\Omega \setminus K_\varepsilon = \partial\Omega$, in particular we can simplify and write

$$w_j(x,y) = \frac{2f_z}{GH}\left(\frac{1}{j\alpha}\right)^2 \left(1 + \oint_{\partial\Omega} \left(\frac{\partial F_j}{\partial \xi}\mathrm{d}\eta - \frac{\partial F_j}{\partial \eta}\mathrm{d}\xi \right)\right), \tag{22}$$

for $[x,y] \in \Omega$,

$$w_j(x,y)\frac{2f_z}{GH}\left(\frac{1}{j\alpha}\right)^2 \oint_{\partial\Omega} \left(\frac{\partial F_j}{\partial \xi}\mathrm{d}\eta - \frac{\partial F_j}{\partial \eta}\mathrm{d}\xi \right) \tag{23}$$

for $[x,y] \in R^2 \setminus (\Omega \cup \partial\Omega)$.

If $w_j(x,y)$ for $j = 1,3,5,\ldots$ are known functions, the stress function $\sigma_{zz}(x,y,z)$ takes the form

$$\sigma_{zz}(x,y,z) = -E_{\text{oed}} \frac{\partial w}{\partial z}(x,y,z) = E_{\text{oed}} \sum_{j=1,3,\ldots} \frac{j\pi}{2H} w_j(x,y) \sin\left(\frac{j\pi z}{2H}\right). \tag{24}$$

5. The phenomenon of influence zone and its estimation

We introduce the subject of considering the distribution of vertical stresses according to Fig. 12. Due to excavation to a certain depth h, the original geostatic stress state, which sets the initial compaction of soil represented by the preconsolidation pressure (see [20,3]), the highest stress level in the soil recorded during the prior loading history, is reduced. Subsequent surcharge at the footing bottom gives further redistribution of the vertical stress. It is assumed that in the region where the vertical effective stress due to surcharge at the footing bottom combined with the reduced geostatic effective stress (by excavation) does not exceed the original geostatic effective stress, the skeleton deformations are negligible. This condition, in our sense, describes the depth of the influence zone H [8,6].

Denote the width of uniform load strip f_z by $2a$, i.e. $\Omega = \{[x,y] : -a < x < a, y \in R\}$. The solution $w(x,y,z)$ of (18) is independent of y : $w = w(x,z)$. There are an infinite number of the ordinary differential equations, together with the boundary and continuity conditions

$$\lim_{|x|\to\infty} w_j(x) = 0,\ w_j \in C^1(R), \quad j = 1,3,\ldots$$

produce the solution

$$w_j(x) = \begin{cases} A_0 + A_1 \cosh(j\alpha x) & \text{for } x \in \langle -a, a\rangle \\ A_2 \exp(-j\alpha|x|) & \text{for } |x| > a, \end{cases}$$

where $A_0 = \frac{2f_z}{GH}\left(\frac{1}{j\alpha}\right)^2$.

Unknown constants A_1, A_2 of integration result from the condition of continuity (of the displacement and its first derivative) at the points of $|x| = a$. Inserting these constants into the above

formula it provides

$$w_j(x) = \frac{2f_z}{GH}\left(\frac{1}{j\alpha}\right)^2 \cdot \begin{cases} 1-\cosh(j\alpha x)\exp(-j\alpha a) & \text{for } |x| \le a \\ \exp(-j\alpha|x|)\sinh(j\alpha a) & \text{for } |x| > a. \end{cases} \quad (25)$$

Hence, the function $w(x, z)$ being in the form of series

$$w(x,z) = \sum_{j=1,3,\ldots} w_j(x)\cos\left(\frac{j\pi z}{2H}\right) \quad (26)$$

solves the problem. The component of the vertical stress function σ_{zz} is evaluated by differentiating $w(x, z)$ with respect to z by terms

$$\begin{aligned}\sigma_{zz}(x,z) &= -E_{\text{oed}}\frac{\partial w}{\partial z}(x,z) = E_{\text{oed}}\sum_{j=1,3,\ldots}\frac{j\pi}{2H}w_j(x)\sin\left(\frac{j\pi z}{2H}\right) \\ &= \frac{4f_z}{\pi}\sum_{j=1,3,\ldots}\frac{1}{j}\sin\left(\frac{j\pi z}{2H}\right) \\ &\quad\cdot\begin{cases} 1-\cosh(j\alpha x)\exp(-j\alpha a) & \text{for } |x| \le a \\ \exp(-j\alpha|x|)\sinh(j\alpha a) & \text{for } |x| > a. \end{cases}\end{aligned}$$

All three series in the above formula can be summed (more in [9]). Finally, the vertical stress σ_{zz} can be written in the form

$$\begin{aligned}\sigma_{zz}(x,z) &= f_z - \frac{f_z}{\pi}\left(\arctan\left(\frac{\sin(\pi z/2H)}{\sinh(\alpha(a-x))}\right)\right. \\ &\quad \left.+\arctan\left(\frac{\sin(\pi z/2H)}{\sinh(\alpha(a+x))}\right)\right), \quad \text{for } |x| \le a \\ \sigma_{zz}(x,z) &= \frac{f_z}{\pi}\left(\arctan\left(\frac{\sin(\pi z/2H)}{\sinh(\alpha(|x|-a))}\right)\right. \\ &\quad \left.-\arctan\left(\frac{\sin(\pi z/2H)}{\sinh(\alpha(|x|+a))}\right)\right), \quad \text{for } |x| > a. \end{aligned} \quad (27)$$

The stress function $\sigma_{zz}(x, z)$ for fixed $z \in \langle 0, H\rangle$ acquires its maximum at the point $x = 0$:

$$\begin{aligned}\max_{x\in R}\sigma_{zz}(x,z) &= \sigma_{zz}(0,z) = f_z - \frac{2f_z}{\pi}\arctan\left(\frac{\sin(\pi z/2H)}{\sinh\alpha a}\right) \\ &= \frac{2f_z}{\pi}\arctan\left(\frac{\sinh\alpha a}{\sin(\pi z/2H)}\right).\end{aligned}$$

The function $\sigma_{zz}(0, z)$ decreases with increasing z. The maximum of the stress function at the bottom ($z = H$) of the influence zone depth is

$$\sigma_{zz}(0,H) = \frac{2f_z}{\pi}\operatorname{arctan\,sinh}\alpha a. \quad (28)$$

The influence zone depth is estimated by means of the quality

$$\sigma_{zz}(0,H) = \gamma h, \quad (29)$$

where γ is the specific weight of soil and h is the depth of the excavation. Comparing the last two identities we obtain

$$\frac{\gamma h}{f_z} = \frac{2}{\pi}\operatorname{arctan\,sinh}\alpha a.$$

Denoting

$$\beta = \frac{2\alpha a}{\pi} = \frac{a}{H}\sqrt{\frac{2-2v}{1-2v}}, \qquad F_{\text{strip}}(\beta) = \frac{2}{\pi}\arctan\left(\sinh\frac{\beta\pi}{2}\right).$$

The above identities give the equation

$$\frac{\gamma h}{f_z} = F_{\text{strip}}(\beta).$$

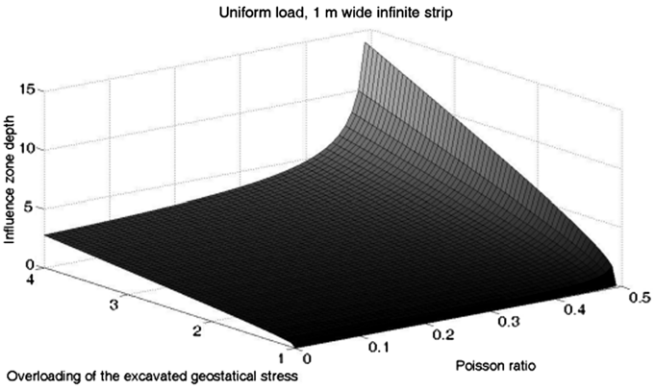

Fig. 13. Progress of influence zone depth of the 1 m wide strip.

Eliminating the influence zone finally yields

$$\begin{aligned}H &= \frac{\pi a}{2}\sqrt{\frac{2-2v}{1-2v}}\frac{1}{\sinh^{-1}\left(\tan\frac{\pi\gamma h}{2f_z}\right)} \\ &= \frac{\pi(2a)}{4}\sqrt{\frac{2-2v}{1-2v}}\frac{1}{\sinh^{-1}\left(\tan\frac{\pi\gamma h}{2f_z}\right)} \\ &= \frac{\pi a}{2}\sqrt{\frac{2-2v}{1-2v}}\frac{1}{\ln\left(\sin\frac{\pi\gamma h}{2f_z}+1\right)-\ln\left(\cos\frac{\pi\gamma h}{2f_z}\right)}.\end{aligned} \quad (30)$$

This closed formula can be effectively used in civil engineering practice. Now we give several comments on the derived identity. First, the influence zone is proportional to the strip load width $2a$. Secondly, the influence zone does not depend on Young's modulus, but there is a significant role for Poisson's ratio. Overloading of the excavation geostatic stress state $f_z/\gamma h$ is the third parameter to be taken into account. All these statements are highlighted in the following Fig. 13.

Similarly, we can estimate the depth of influence zone in the case of rectangular footings. Let us introduce the function

$$\begin{aligned}F(\beta) &= \frac{2}{\pi}\left(\arctan\frac{\beta\pi b}{2a}+\arctan\frac{\beta\pi}{2}\right) \\ &\quad -\frac{4}{\pi^2}\int_0^1\frac{1}{\sqrt{\left(\frac{a}{b}\right)^2+1-t^2}}\operatorname{arctan\,sinh} \\ &\quad\times\left(\frac{\frac{\beta\pi b}{2a}}{\sqrt{1-t^2}}\sqrt{\left(\frac{a}{b}\right)^2+1-t^2}\right)\mathrm{d}t - \frac{4}{\pi^2} \\ &\quad\times\int_0^1\frac{1}{\sqrt{\left(\frac{b}{a}\right)^2+1-t^2}}\operatorname{arctan\,sinh} \\ &\quad\times\left(\frac{\frac{\beta\pi}{2}}{\sqrt{1-t^2}}\sqrt{\left(\frac{b}{a}\right)^2+1-t^2}\right)\mathrm{d}t, \\ \beta &= \frac{2\alpha a}{\pi} = \frac{a}{H}\sqrt{\frac{2-2v}{1-2v}}.\end{aligned} \quad (31)$$

The function $F(\beta)$ describes the maximum layer bottom vertical stress $\sigma_z(0, 0, H)$ by the unit uniform load acting in the rectangular region $2a \times 2b$. The depth of the influence zone is described by the point where the vertical stress due to surcharge reaches the value γh. The maximum stress below the centre of rectangle at the depth H can be then expressed in the following form

$$\sigma_z(0,0,H) = f_z F(\beta) = \gamma h. \quad (32)$$

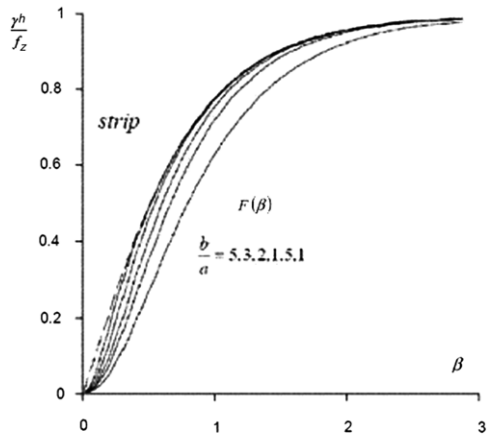

Fig. 14. Courses of $F(\beta)$ function.

As the value of preconsolidation γh and the level of surcharge f_z are known, the value β is obtained as the inverse of the function $F(\beta)$. The following formula describes this statement and the idea as to how to calculate the depth of the influence zone

$$\frac{\gamma h}{f_z} = F(\beta) \rightarrow \beta = \frac{a}{H}\sqrt{\frac{2-2v}{1-2v}} \rightarrow H. \tag{33}$$

Functions $F(\beta)$ for some quotients a/b are presented in Fig. 14.

6. Verification of derived formulas using FEM ADINA solutions

This part focuses on the comparison between results obtained using the formulas described above and results obtained from the finite element code ADINA (Automatic Dynamic Incremental Nonlinear Analysis). At first the infinite strip (line for an infinitezimal a) load line load problem was selected for comparison and the values of $\sigma_{zz}(0, H)$ are compared. The size of the numerical model in terms of depth equals the selected depth of the influence zone, i.e. H.

Let us first restate the derived formulas for $\sigma_{zz}(0, H)$ in the case of an infinite strip load.

$$\sigma_{zz}(0, H) = \frac{2f_z}{\pi} \operatorname{arctan\,sinh} \alpha a$$

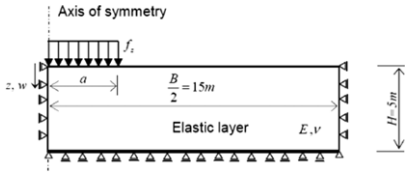

Fig. 15. Scheme of the tested example.

where:

H …depth of influence zone,

f_z …value of the strip load,
ν …Poisson's ratio,
a …half of the strip width,
$\alpha \ldots \alpha = \frac{\pi}{2H}\sqrt{\frac{2-2\nu}{1-2\nu}}$.

For the FEM analysis, the following assumptions were used.

- 1 degree of freedom for nodes (z-direction)
- Plain strain
- Isotropic elastic material
- Symmetry—only one half of the model
- Software ADINA (Automatic Dynamic Incremental Nonlinear Analysis).

Shape of the FE mesh, type of the FE are subjected to change to observe the influence on the results.

The tested example has the following details:
Infinite strip line load $f_z = 100\,000$ kN/m^2.
Infinite line load $f_z = 100\,000$ kN/m.
Depth of influence zone $H = 5$ m.
Material properties are $E = 75$ GPa; ν varies from $ny = 0.3$.
Model width $B = 30$ m (15 m using symmetry).

The main reason for applying such a high and nearly unreal magnitude of load was to get sufficient digital output in the computer code. The geometry of the described example is clear from Fig. 15.

Table 4 shows the results obtained from numerical analysis for five different shapes of the FE mesh. Three setups had coarse mesh with different points of densification. Two other setups had fine mesh. The mesh shapes tested are clear from Fig. 16. For every mesh shape four types of FE were used, i.e. triangle with 7 and 3 nodes and quad with 9 and 4 nodes. The details for the used FE types can be found in [21]. An analytical solution gives $\sigma_{zz}(0.5) =$ 18 708 kPa.

Table 4
Numerical results for varying FE mesh and types of FE.

Mesh type	FE type	FE area (m^2)	Number of DOF	Number of FEM	σ_{zz} (kPa)	Relative diff. (%)
Type 1	9-Node quad	0.06875	1559	374	18 665	−0.23
	7-Node triangle	0.034375	2259	724	18 678	−0.16
	4-Node quad	0.06875	406	374	18 621	−0.47
	3-Node triangle	0.034375	406	724	18 765	0.31
Type 2	9-Node quad	0.0187	1559	374	18 687	−0.11
	7-Node triangle	0.00935	2259	724	18 694	−0.08
	4-Node quad	0.0187	406	374	18 657	−0.27
	3-Node triangle	0.00935	406	724	18 757	0.26
Type 3	9-Node quad	0.0125	1559	374	18 698	−0.06
	7-Node triangle	0.00625	2259	724	18 699	−0.05
	4-Node quad	0.0125	406	374	18 689	−0.10
	3-Node triangle	0.00625	406	724	18 912	1.09
Type 4	9-Node quad	0.0825	3731	900	18 638	−0.38
	7-Node triangle	0.04125	5531	1800	18 659	−0.26
	4-Node quad	0.0825	966	900	18 568	−0.75
	3-Node triangle	0.04125	966	1800	18 817	0.58
Type 5	9-Node quad	0.01155	3709	900	18 691	−0.09
	7-Node triangle	0.005775	5455	1773	18 697	−0.06
	4-Node quad	0.01155	955	900	18 672	−0.20
	3-Node triangle	0.005775	955	1773	18 729	0.11

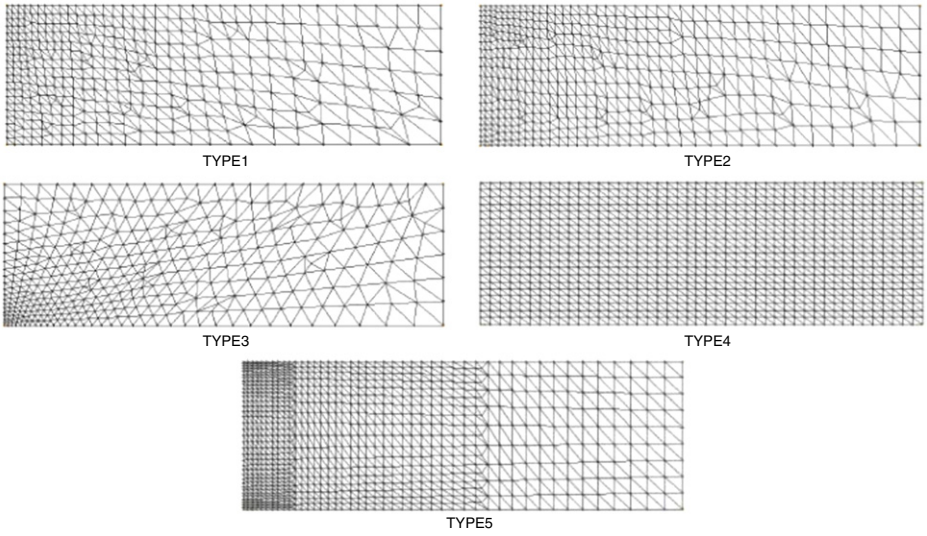

Fig. 16. Shapes of FE mesh.

Table 5
Numerical results.

1/2 uniform load width (m)	0	0.5	1	2	4	8
Poisson's ratio	$\sigma_{zz}(0, H)$ (kPa)					
0.05	14 531.1	14 412.0	14 053.9	12 853.8	9 959.04	6044.0
0.15	15 585.0	15 437.8	15 000.4	13 565.1	10 269.9	6091.8
0.25	17 322.0	17 118.7	16 528.5	14 661.8	10 702.9	6147.7
0.3	18 709.0	18 453.2	17 720.4	15 472.4	10 988.6	6177.8
0.35	20 818.0	20 464.7	19 479.0	16 596.9	11 339.0	6207.5
0.4	24 495.8	23 922.6	22 388.4	18 273.6	11 767.9	6233.1

Table 6
Analytical results.

1/2 uniform load width (m)	0	0.5	1	2	4	8
Poisson's ratio	$\sigma_{zz}(0, H)$ (kPa)					
0.05	14 529.7	14 405.1	14 049.9	12 851.1	9 958.2	6043.6
0.15	15 583.9	15 430.5	14 996.2	13 562.5	10 269.1	6091.6
0.25	17 320.5	17 110.7	16 524.1	14 659.3	10 702.4	6147.6
0.3	18 708.3	18 444.7	17 715.8	15 470.0	10 988.2	6177.8
0.35	20 816.7	20 455.3	19 474.1	16 594.7	11 338.6	6207.5
0.4	24 494.9	23 912.0	22 383.3	18 271.7	11 767.7	6233.1

Another group of numerical tests were performed for the infinite stripe load problem with varying width of the strip (a = 0–8 m) and Poisson's ratio (from 0.05 to 0.4). The strip load was width dependent so in total it remains the same, i.e. f_z = 100 000 kN/m^2 for a = 0.5 m; f_z = 50 000 kN/m^2 for a = 1.0 m; etc.

The results obtained are presented in Tables 5 and 6. The presented results show very good agreement. The differences are smaller than 0.1% for this range of Poisson's ratio. In all presented results, we keep the geotechnical convention in the stress values, i.e. positive stress value means pressure while the negative stress value is tension.

The results obtained from numerical analysis are generally in very good agreement with the results derived from the presented formulas. We can actually now use the described theory for checking the accuracy of newly built FE codes and FE types. More tests were performed with other codes and types of problems and results can be found in [22].

7. Conclusion

The contribution summarized research activity carried out at CTU in Prague, Czech Republic, and UnB Brasilia, Brazil. Within the scope of interest were mainly preconsolidation, a special kind of soil memory, and its effect on the soil upper structure interaction. In the laboratory the significant influence of over-consolidation on pore pressure evolution during isotropic consolidation with the triaxial test apparatus was considered. Vice versa, employing the genetic algorithms the soil parameters can be effectively investigated; namely initial void ratio and preconsolidation effective mean pressure. Concerning in situ testing we analyzed the working diagrams of piles. In collaboration with UnB Brazil, provider of in situ tests, we observed also the significant effect of preconsolidation in the pile heel. Robust theory and derivation of many analytical formulas were accomplished and consequently implemented to the computer code to capture the relevant result of the pile behavior. Also we would like to underline the idea of influence zone estimation. The close formula for its estimation can be effectively used in civil engineering practice as it gives immediately the value of influence zone depth. As it was derived from the load acting in infinite strips the value of the influence zone depth is just almost a little bit overestimated. The present close formula was verified against the numerical code ADINA, to enhance its credit. In general, the benefit of a semi-analytical solution can be found in what follows. Input parameters

are very easily estimated and also they are intelligible for civil engineers. Calculation is very fast and it gives relevant results. Analytical and semi-analytical solutions significantly save time for designers in contrast to pure numerical methods.

Otherwise, if it is necessary, the semi-analytical solution gives a very good starting point for future numerical fine tuning. Technical knowledge based on the presented results and theory was implemented in the computers codes, namely GEO5.

Acknowledgements

The research presented in this lecture has been carried out with financial support received by the author from Contract of the Ministry of Education, Youth and Sports of the Czech Republic no. MSM 6840770001 and the Czech Science Foundation (grants No. 103/08/1119 and 103/08/1617).

References

[1] Asaoka A, Nakano M, Noda T. "Super loading yield" surface concept for the saturated structured soils. In: Cividini A (Ed.), NUMGE98. Udine (Italy); 1998. p. 233–42.
[2] Bowles JE. Foundation analysis and design. New York: McGraw-Hill; 1966.
[3] Terzaghi K, Peck RB, Mesri Ch. Soil mechanics in engineering practice. Chichester (NY): Wiley; 1996.
[4] Janda T, Kuklík P, Šejnoha M. Mixed experimental and numerical approach to evaluation of material parameters of clayey soils. Int J Geomech 2004;4(3): 199–206.
[5] Matouš K, Lepš M, Zeman J, Šejnoha M. Applying genetic algorithms to selected topics commonly encountered in engineering practice. Comput Methods Appl Mech Engrg 2000;119:1600–20.
[6] Kuklík P, Kopáčková M. Comparison of elastic layer solution with Boussinesq half space solution. Stavební Obzor 2004;6:171–5 [in Czech].
[7] Kuklík P. Several comments on influence zone depth progress in deep hole foundations. In: Proceedings of the geoShanghai conference 2006. 2006.
[8] Daloglu AT, Ozgan K. The effective depth of soil stratum for plates resting on elastic foundation. Struct Eng Mech 2004;18(2):263–76.
[9] Gradschtein IS, Rizhik IM. Tables of integrals, sums, series and product. Moscow. 1963 [in Russian].
[10] Kotrasová K. Influence of category of sub-soil on liquid storage circular tanks during earthquake. In: 12th international scientific conference. 2009.
[11] Kuklík P, Šejnoha M, Mareš J. Dimensional reduction applied to specific problems of consolidation. In: Application of numerical methods to geotechnical problems. Wien: Springer; 1998. p. 337–46.
[12] Kvasnička V. Augmented simulated annealing adaption of feed-forward neural networks. Neural Netw World 1994;3:67–80.
[13] Kuklík P, Mares J, Šejnoha M. The structural strength of soil from the isotropic consolidation point of view. In: Wang CM, Lee KH, Ang KK (Eds.), APCOM 99. Singapore. vol. 2. 1999. p. 797–802.
[14] Cunha RP, Jardim NA, Pereira JHF. In situ characterization of a tropical porous clay via dilatometer tests. In: Geo-congress 99 on behavioral characteristics of residual soils. ASCE Pub. 92. Charlotte. 1999. p. 113–22.
[15] Cunha RP, Kuklík P. Numerical evaluation of pile foundations in tropical soils of the federal district of Brazil by means of a semi-analytical mathematical procedure. Solos e Rochas, Suelos y Rocas, Soils and Rocks 2003;26(2):167–82.
[16] Rektorys K. Survey of applicable mathematics. London: ILIFFE Books; 1995.
[17] Shufrin I, Eisenberger M. In-plane vibrations of rectangular plates with rectangular cutouts. In: Proceedings of the EPMESC X. 2006 [in China].
[18] Fajman P, Šejnoha J. A simplified approach to time-dependent subsoil-structure interaction. Comput Struct 2007;85:1514–23.
[19] Mistrikova Z, Jendzelovsky N. Soil-axisymmetric slab interaction for different models of subsoil. Civ Environ Eng 2009;5(1):18–28 [in Slovak].
[20] Lewis RW, Schrefler BA. The finite element method in static and dynamic deformation and consolidation of porous media. Chichester (NY): Wiley; 1998.
[21] Bathe KJ. Finite elements procedures. New Jersey: Prentice-Hall, Inc.; 1996.
[22] Kuklík P, Kopáčková M, Brouček M. Elastic layer theory and geomechanics. 1st ed. Praha: CTU Publishing House; 2009. p. 109.